DEVELOPMENT AND IMPLEMENTATION OF INTEGRATED q-PROFILE+β_N FEEDBACK CONTROL STRATEGIES FOR ADVANCED SCENARIOS IN EAST

E. SCHUSTER, H. WANG, Z. WANG
Lehigh University
Bethlehem, Pennsylvania 18015, USA
Email: schuster@lehigh.edu

Y. HUANG, Z. LUO, B. XIAO, Q. YUAN
Institute of Plasma Physics, Chinese Academy of Sciences
Hefei, China

J. BARR, D.A. HUMPHREYS, A.W HYATT, M.L. WALKER, W.P. WEHNER
General Atomics
San Diego, California, USA

Abstract

Experiments on integrated q-profile and β_N closed-loop control have been recently conducted for the first time ever in EAST. In order to achieve advanced modes of operation, characterized by confinement improvement and possible steady-state operation, it is critical to count with robust control capabilities for shaping the spatial profile of the toroidal current density, or equivalently the safety factor q or the gradient of the poloidal magnetic flux, and simultaneously regulating a measure of the plasma internal energy such as β_N. Several model-based and non-model-based controllers have been designed with the capability of either regulating several points of the q profile, minimizing the integrated squared error between actual and target profiles, or controlling integral properties such as the internal plasma inductance l_i, while at the same time regulating β_N. To enable the experimental testing of many of these controllers, a general framework for real-time feedforward + feedback control of magnetic and kinetic plasma profiles and scalars has been implemented in the EAST Plasma Control System (PCS). Moreover, critical actuators including the ohmic coils, two Lower Hybrid Wave (LHW) sources, and four Neutral Beam Injection (NBI) sources have been placed under the PCS command. The q profile at 11 points and β_N have been reconstructed in real-time by pEFIT, an equilibrium reconstruction code exploiting the massively parallel processing cores of graphic processing units (GPUs). These initial experiments show successful regulation of the q profile at several points. Further development work, which includes the increase of the number of actuators, the improvement of the quality of the real-time plasma-state reconstruction, and the enhancement of the plasma-response models used for control design, is planned to make this control capability a routine enabler of long-pulse, disruption-free, high-performance operation in the EAST tokamak.

1. Introduction

Regulation of the q-profile via feedback control has been recently demonstrated in EAST in both L-Mode and H-mode experiments. Extensive studies have shown that the q-profile, which is closely related to poloidal magnetic flux profile, is a key factor to achieving advanced-tokamak operating scenarios that are characterized by improved confinement and the non-inductive sustainment of the plasma current necessary for steady-state operation. A general framework for real-time feedforward + feedback control of magnetic and kinetic plasma profiles as well as scalars has been implemented in the EAST Plasma Control System (PCS). Moreover, a first-principles-driven, control-oriented model of the poloidal magnetic flux profile and internal energy evolutions has been used to design feedforward [1] and feedback [2, 3] model-based control algorithms. As it is the case in this work, this model has also been used to tune non-model-based control algorithms and to debug controller implementations in the PCS, both in closed-loop simulations. Several of these proposed controllers have been tested successfully in reference tracking and disturbance rejection experiments in EAST. These experiments constitute the first time ever closed-loop q-profile regulation has been successfully achieved in EAST.

The controllers have the capability of either regulating several points of the q profile, minimizing the integrated squared error between actual and target profiles, or controlling integral properties such as the internal plasma inductance l_i. Moreover, the controllers can simultaneously regulate β_N, which is another plasma property playing a key role in the access to high-performance, MHD-stable modes of operation. This level of controllability has been achieved in EAST by placing several critical actuators under the PCS command, namely the ohmic coils, two Lower Hybrid Wave (LHW) sources, and four Neutral Beam Injection (NBI) sources. The so-called Profile Control category recently implemented in the EAST PCS, which houses the q-profile+β_N control algorithms, does not directly control these actuators. Instead, it sends requests for the needed total plasma current and non-inductive

powers to the different actuator categories. To enable the use of NBI power for q-profile+β_N control, a pulse-width-modulation algorithm was also implemented in the PCS to convert the power requests from the Profile Control category into on/off time commands for the beams. While this actuator mechanism proved to be too powerful for smooth β_N regulation in low-energy discharges, it is anticipated that it could play an important role after refinement. Both the q profile at 11 points and β_N are passed to the Profile Control category by pEFIT [4], an equilibrium reconstruction code exploiting the parallel-processing capability of graphic processing units (GPUs).

This paper is organized as follows. Efforts towards the development of a control-oriented model for the prediction of the response of the q profile and β_N to the different actuators in EAST is summarized in Section 2. An overview of the control-design problem is provided in Section 3. Details on the implementation of the developed control algorithms in the EAST PCS is discussed in Section 4. Some initial experimental results are presented in Section 5. Conclusion and potential future work are stated in Section 6.

2. Poloidal Magnetic Flux and Energy Evolution Models

2.1. Poloidal Magnetic Flux Dynamics

The evolution of the poloidal stream function (ψ), which is related to the poloidal magnetic flux Ψ as $\psi \triangleq \Psi/(2\pi)$, is governed by the magnetic diffusion equation (MDE) [5],

$$\frac{\partial \psi}{\partial t} = \frac{\eta(T_e)}{\mu_0 \rho_b^2 \hat{F}^2} \frac{1}{\hat{\rho}} \frac{\partial}{\partial \hat{\rho}} \left(\hat{\rho} D_\psi \frac{\partial \psi}{\partial \hat{\rho}} \right) + R_0 \hat{H} \eta(T_e) \frac{\left\langle \bar{j}_{NI} \cdot \bar{B} \right\rangle}{B_{\phi,0}}, \tag{1}$$

with two given boundary conditions,

$$\left. \frac{\partial \psi}{\partial \hat{\rho}} \right|_{\hat{\rho}=0} = 0, \qquad \left. \frac{\partial \psi}{\partial \hat{\rho}} \right|_{\hat{\rho}=1} = \frac{k}{2} I_p(t), \tag{2}$$

and where $D_\psi(\hat{\rho}) = \hat{F}(\hat{\rho})\hat{H}(\hat{\rho})\hat{G}(\hat{\rho})$, $k = -\frac{\mu_0}{\pi} \frac{R_0}{\hat{G}(1)\hat{H}(1)}$, and I_p is the plasma current. $\hat{F}$, $\hat{G}$ and $\hat{H}$ are spatially varying geometric factors pertaining to the magnetic configuration of a particular plasma equilibrium, μ_0 is the vacuum permeability, $\langle \cdot \rangle$ denotes a flux-surface average, and t denotes the time. In this work, the spatial coordinate is chosen as the mean effective minor radius, $\rho \triangleq \sqrt{\Phi/(B_{\phi,0}\pi)}$, where $B_{\phi,0}$ is the vacuum toroidal magnetic field at the major radius, R_0, and Φ is the toroidal magnetic flux. A normalized version of ρ is given by $\hat{\rho} \triangleq \rho/\rho_b$, where ρ_b is the mean effective minor radius of the last-closed magnetic-flux surface. Control-oriented models for the electron temperature and density (T_e and n_e), ion temperature and density (T_i and n_i), plasma resistivity η, and non-inductive current-drive $\frac{\langle \bar{j}_{NI} \cdot \bar{B} \rangle}{B_{\phi,0}}$ are needed for closure of the MDE [6, 7].

A tight coupling between the electron and ion species in the plasma is assumed in this work, i.e. $n_e \propto n_i$ and $T_e \propto T_i$. In particular, electron and ion densities and temperatures are treated as identical in the model presented in this section but this condition could be relaxed. The electron density $n_e(\hat{\rho}, t)$ is modeled as $n_e(\hat{\rho}, t) = n_e^{prof}(\hat{\rho})\bar{n}_e(t)$, where n_e^{prof} is a reference electron density profile and $\bar{n}_e(t)$ is the line-averaged electron density. The electron temperature is modeled as $T_e(\hat{\rho}, t) = T_e^{prof}(\hat{\rho}) I_p(t)^\alpha P_{tot}(t)^\gamma \bar{n}_e(t)^\kappa$, where T_e^{prof} is a reference electron temperature profile, P_{tot} represents the total injected power, and α, γ, κ are positive scaling factors. The plasma resistivity $\eta(T_e)$ is assumed to scale with the electron temperature as $\eta(\hat{\rho}, t) = \frac{k_{sp}(\hat{\rho}) Z_{eff}}{T_e(\hat{\rho}, t)^{3/2}}$, where k_{sp} is a spatial profile and Z_{eff} is the effective atomic number of the ion species in the plasma.

The non-inductive current drive (j_{NI}) is the sum of the self-generated bootstrap current (j_{BS}) and the currents driven by each of the auxiliary sources such as Lower Hybrid Wave (j_{LH}) and Neutral Beam Injection (j_{NBI}), i.e.

$$\frac{\langle \bar{j}_{NI} \cdot \bar{B} \rangle}{B_{\phi,0}} = \sum_{i=1}^{4} \frac{\langle \bar{j}_{NBI_i} \cdot \bar{B} \rangle}{B_{\phi,0}} + \sum_{i=1}^{2} \frac{\langle \bar{j}_{LH_i} \cdot \bar{B} \rangle}{B_{\phi,0}} + \frac{\langle \bar{j}_{BS} \cdot \bar{B} \rangle}{B_{\phi,0}}. \tag{3}$$

In this work, we consider six of EAST's non-inductive current sources, namely four NBI (NBI1L, NBI1R, NBI2L, NBI2R) and two LHW (2.45 GHz, 4.60 GHz) current-drive sources. Each auxiliary source $\langle \bar{j}_x \cdot \bar{B} \rangle / B_{\phi,0}$, where $x \in \{NBI_i, LH_i\}$, is modeled by the product of a reference deposition profile $j_i^{dep}(\hat{\rho})$, an efficiency term $T_e(\hat{\rho}, t)^\delta / n_e(\hat{\rho}, t)$ where δ is 0.5 for NBI and 1 for LHW, and the power associated with the source $P_x(t)$, i.e.

$$\frac{\langle \bar{j}_x \cdot \bar{B} \rangle}{B_{\phi,0}}(\hat{\rho}, t) = j_x^{dep}(\hat{\rho}) \frac{T_e(\hat{\rho}, t)^\delta}{n_e(\hat{\rho}, t)} P_x(t). \tag{4}$$

The bootstrap current model is based on [8], which with the electron-ion tight coupling assumption reduces to

$$\frac{\langle \bar{j}_{BS} \cdot \bar{B} \rangle}{B_{\phi,0}}(\hat{\rho}, t) = \frac{R_0}{\hat{F}} \left(\frac{\partial \psi}{\partial \hat{\rho}} \right)^{-1} \left[\mathcal{L}_1 T_e \frac{\partial n_e}{\partial \hat{\rho}} + \mathcal{L}_2 n_e \frac{\partial T_e}{\partial \hat{\rho}} \right], \tag{5}$$

where the spatial functions $\mathcal{L}_1(\hat{\rho})$ and $\mathcal{L}_2(\hat{\rho})$ depend on the magnetic configuration of a particular equilibrium.

The safety factor q and the plasma internal inductance l_i, which is an integral function of q, and therefore of $\theta \triangleq \partial\psi/\partial\hat{\rho}$, usually employed as a measure of the q profile broadness or peakedness, are defined respectively as

$$q(\hat{\rho},t) = -\frac{d\Phi}{d\Psi} = -\frac{d\Phi/d\rho}{d\Psi/d\rho} = -\frac{B_{\phi,0}\rho_b^2\hat{\rho}}{\partial\psi/\partial\hat{\rho}}, \tag{6}$$

$$l_i = \frac{8\pi^2}{\mu_o{}^2 R_o{}^2 I_p{}^2}\int_0^1 \hat{\rho}\hat{G}\hat{H}\theta^2 d\hat{\rho}. \tag{7}$$

It is clear from (6) and (7) that the dynamics of both q and l_i are determined by the dynamics of ψ.

2.2. Plasma Stored Energy Dynamics

The evolution of the plasma stored energy density can be approximately modeled by the balance equation

$$\frac{dW}{dt} = -\frac{W}{\tau_E(t)} + P_{tot}(t) \tag{8}$$

where τ_E is the global energy confinement time

$$\tau_E \propto I_p(t)^{\alpha} P_{tot}(t)^{(\gamma-1)} \bar{n}_e(t)^{(1+\kappa)}. \tag{9}$$

The model used for τ_E is based on the $IPB98(y,2)$ scaling law [9], which results in $\alpha = 0.96$, $\gamma = 0.27$, and $\kappa = -0.6$. The total injected power is defined as $P_{tot} = P_{aux} + P_{ohm} - P_{rad}$, where $P_{aux} \triangleq \sum_{i=1}^{4} P_{NBI_i} + \sum_{i=1}^{2} P_{LH_i}$ is the total auxiliary heating/current-drive (H&CD) power, P_{ohm} is the ohmic power, and P_{rad} is the radiation power.

The normalized plasma beta, β_N, is a measure of the ratio between the kinetic energy in the plasma and the magnetic energy used for plasma confinement. It is related to the plasma stored energy W through

$$\beta_N = \frac{(2/3)W/V_p}{B_{\phi,0}{}^2/(2\mu_0)}\frac{aB_{\phi,0}}{I_p}, \tag{10}$$

where a is the minor radius of the plasma, and V_p is the plasma volume.

2.3. Model Validation via Open-loop Plasma-response Characterization Experiments

Several plasma-response characterization experiments were conducted before the q-profile+β_N feedback-control experiments. In these open-loop experiments, plasma-response data was generated by exciting the plasma through the different available actuators. As an example, Fig. 1 shows the typical response of the q profile at two spatial locations ($\hat{\rho} \in [0.1, 0.3]$) in response to open-loop excitation of P_{LH2} (4.6 GHz LHW source power) during the flattop phase in shot #77643. This data was used to tailor the control-oriented model introduced earlier in this section to EAST. This model was used in this work to optimize the gains of the fixed-structure controller proposed in Section 3 and to test the PCS implementation of these controllers in closed-loop Simserver simulations as explained in Section 4.6.

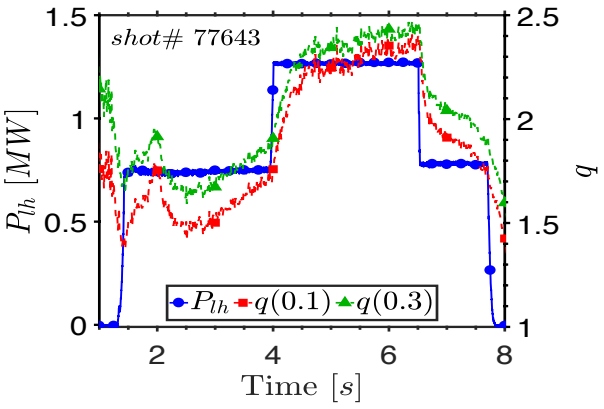

Figure 1: *Response of q-profile to LHW in EAST shot 77643.*

3. Control Design Problem

Active control of both the q profile and β_N (or the plasma energy W) based on a combined feedforward+feedback scheme has the potential of playing a crucial rule at EAST in achieving and sustaining advanced scenarios of interest and in facilitating investigation of their properties. The feedforward component of the control solution can be obtained either by trial and error based on the physics operator's expertise or by embedding fast control-oriented predictive models like the one introduced in Section 2 in a nonlinear optimization algorithm [1]. The result of this scenario-development work is a feedforward control policy (set of actuator waveforms) that under ideal conditions steers the plasma state through the tokamak operating space from a particular initial condition to a predefined target q profile and β_N (or W) value at a given time, while respecting plasma state and actuator constraints. However, variability in the plasma startup and tokamak wall conditions, plasma disturbances, and uncertainties in the model used for the optimization can lead to poor performance with feedforward control alone. Therefore, feedforward control must be complemented with feedback control to add robustness and improve control performance.

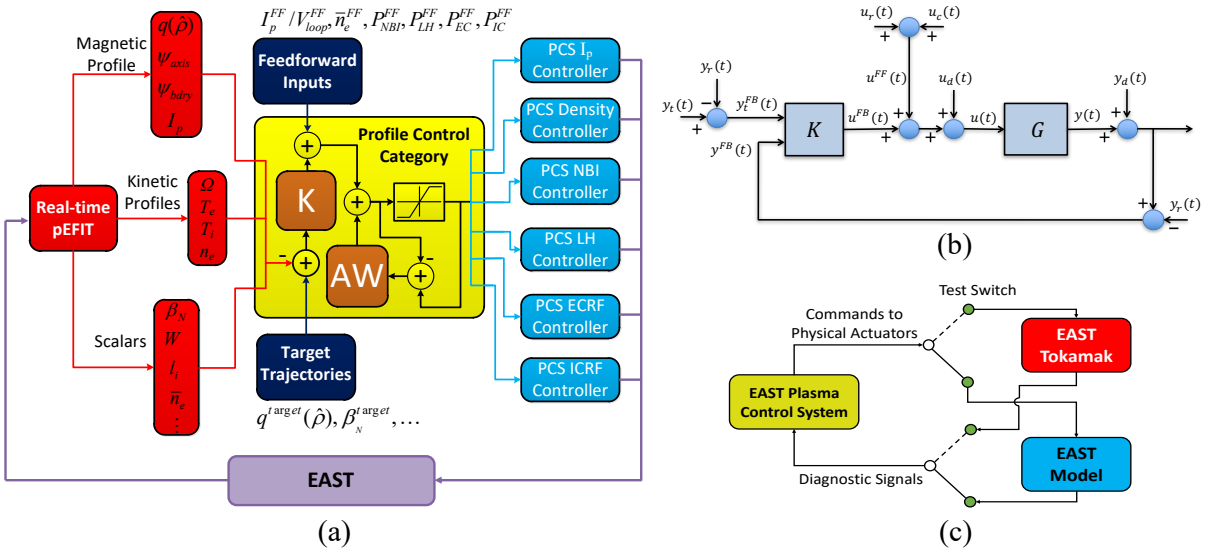

Figure 2: *(a) Architecture of Profile Control category; (b) General control-system configuration; (c) Simulation Simserver.*

The overall objective of the work presented in this paper was to design, implement, and experimentally test feedback control algorithms for q-profile and β_N regulation for the first time at EAST. Due to the high-dimensionality, nonlinearity, and magnetic-kinetic coupling of this control problem, control-oriented response models like the one introduced in Section 2 can play a critical role in the synthesis of the feedback control algorithms. These models can be embedded in the control synthesis procedure [2, 3] or can be used to select and optimize the gains of control algorithms with fixed structures. In this work, the latter approach has been followed. The actuators considered in this work were the total plasma current I_p, the power of the 2.45 GHz LWH source P_{LH1}, the power of the 4.6 GHz LHW source P_{LH2}, the power of individual co-current NBI sources (P_{NBI1} (NBI1L), P_{NBI2} (NBI1R)), and the power of individual counter-current NBI sources (P_{NBI3} (NBI2L), P_{NBI4} (NBI2R)). The LHW sources were used mainly as current drives and the NBI sources were used mainly as heating mechanisms. Due to limited actuation capabilities, the experiments reported in this paper focused on regulating the value of the safety factor q at discrete points in space in combination in some cases with β_N regulation.

The feedback (FB) control algorithms tested in the experiments reported in this paper used a proportional-integral-derivative structure given by

$$u^{FB}(t) = K_P e(t) + K_I \int_o^t e(t) + K_D \frac{de(t)}{dt} \tag{11}$$

where $u^{FB} = [I_p^{FB}\ P_{LH1}^{FB}\ P_{LH2}^{FB}\ P_{NBI1}^{FB}\ P_{NBI2}^{FB}\ P_{NBI3}^{FB}\ P_{NBI4}^{FB}]^T$, $e = [q(0.1) - q^{tgt}(0.1)\ \ q(0.5) - q^{tgt}(0.5)\ \ q(0.9) - q^{tgt}(0.9)\ \ \beta_N - \beta_N^{tgt}]^T$, and K_P, K_I, K_D are gain matrices optimized in simulations based on the control-oriented model introduced in Section 2. The superscript *tgt* denotes target values for the to-be-controlled plasma properties.

4. Implementation in the EAST PCS

4.1. Profile Control Category

By exploiting the fact that the DIII-D PCS and the EAST PCS share the same platform, the Profile Control category originally developed by Lehigh University in collaboration with DIII-D was imported from DIII-D into EAST and tailored to EAST's diagnostics and actuators. At present, the Profile Control category implemented in the EAST PCS has the capability of executing different control algorithms for the simultaneous regulation of one plasma magnetic profile and and up to two selected plasma kinetic profiles. In addition, this category has the capability of also regulating up to four selected plasma scalars simultaneously. Fig. 2(a) shows the overall architecture of this category, which allows for the implementation of combined feedforward+feedback control approaches. The feedforward control signals are calculated off-line and are denoted as $(\cdot)^{FF}$. The feedback control signals are the outputs of the selected controller, like the one introduced in Section 3, and are denoted as $(\cdot)^{FB}$. The coordinates of the magnetic and kinetic profiles are the normalized effective minor radius $\hat{\rho}$, which is discretized evenly in space with 21 and 11 nodes, respectively. The set of possible magnetic profiles includes q, the rotational transform ($\iota = 2\pi/q$), ψ, and the gradient of ψ ($\theta = \partial\psi/\partial\hat{\rho}$). The set of possible kinetic profiles includes the toroidal angular velocity (Ω), T_e, T_i, and n_e. The set of possible scalars includes β_N, W, the internal inductance l_i, the line-average electron density ($\bar{n}_e$), the minimum value of the safety factor profile (q_{min}), the safety factor profile at the magnetic axis (q_0), and the safety factor profile at the plasma edge (q_{95}). A sampling time of 10 milliseconds was used for the Profile Control category in this work.

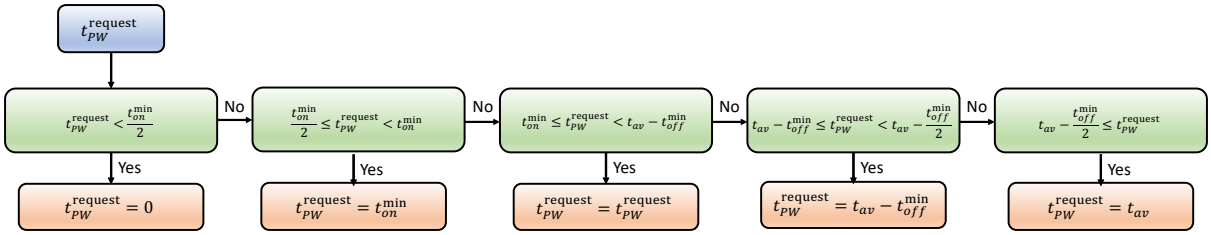

Figure 3: *Power width modulation (PWM) algorithm satisfying minimum on/off time constraints.*

4.2. General Configuration of the Profile Control Algorithms

Fig. 2(b) illustrates the overall control-system configuration implemented in the Profile Control category. The overall input of dimension m for the plant G (EAST) can be written as

$$u = u^{FF} + u^{FB} + u_d, \tag{12}$$

where u^{FB} denotes the feedback component provided by the selected control algorithm K, u_d denotes the input disturbance vector that can be arbitrarily defined for controller testing purposes, and u^{FF} denotes the feedforward component, which in turns can be written as $u^{FF} = u_r + u_c$, where u_r denotes the input reference vector and u_c denotes a potential feedforward compensator. An output disturbance vector y_d can be added to the overall plant output y of dimension p for controller testing purposes. An output reference vector y_r, usually associated with the input reference vector u_r, can be subtracted from the disturbed output $y + y_d$, which makes the input to the feedback controller equal to

$$y^{FB} = y + y_d - y_r. \tag{13}$$

Similarly, the output reference vector y_r can be subtracted from the output target vector y_t, which makes the target passed to the feedback controller equal to

$$y_t^{FB} = y_t - y_r. \tag{14}$$

Both u_r and y_r can play important roles in the implementation of controllers designed based on models linearized around a reference trajectory. The vectors u_r, u_d, y_r, y_d, and y_t must be uploaded to the PCS before each discharge either as text files to be read by the category or as waveforms in the user interface of the category.

4.3. State Feedback Controller

One of the control algorithms implemented in the Profile Control category has a general linear state-space representation. This feedback control algorithm is written in discrete-time state-space form as

$$x_{k+1} = Ax_k + B\begin{bmatrix} y_t - y_r \\ y + y_d - y_r \end{bmatrix}_k, \qquad u_k^{FB} = Cx_k + D\begin{bmatrix} y_t - y_r \\ y + y_d - y_r \end{bmatrix}_k, \tag{15}$$

where the vector x of dimension n represents the state of the feedback controller. It is very important to realize at this point that after time discretization the proposed controller (11) can indeed be implemented in the Profile Category by using this linear discrete-time state-space representation.

4.4. Anti-windup Compensator

The controller (15) is complemented by an anti-windup compensator in discrete-time state-space form given by

$$x_{k+1}^{aw} = A_{aw}x_k^{aw} + B_{aw}\left[sat(u) - u\right]_k, \qquad s_{k+1} = C_{aw}x_k^{aw} + D_{aw}\left[sat(u) - u\right]_k, \tag{16}$$

where the vector x^{aw} of dimension n_{aw} represents the state of the anti-windup compensator and the vector s of dimension $q_{aw} = m$ denotes the output of the anti-windup compensator. When the anti-windup is turned on, the controller output u is modified by the anti-windup output as $u = u^{FF} + u^{FB} + u_d + s$. The saturation function is defined as $sat(\cdot) = (\cdot)$ if $(\cdot)^{min} \le (\cdot) \le (\cdot)^{max}$, $sat(\cdot) = (\cdot)^{min}$ if $(\cdot) < (\cdot)^{min}$, and $sat(\cdot) = (\cdot)^{max}$ if $(\cdot) > (\cdot)^{max}$.

4.5. Pulse Width Modulation for the Command of NBI Power

The NBI system has a preset power output P_{NBI}^{max} for each beam. Since the command of the NBI system is on/off, modulation is needed to achieve the requested average power output P_{NBI} without violating the minimum on-time, which is the time that the NBI needs to be kept on before shutting it off, and the minimum off-time, which is the time that the NBI needs to be kept off before turning it on. In this work, pulse width modulation (PWM) is used to convert the requested NBI power P_{NBI} to on/off commands. The PWM logic shown in Fig.3 guarantees that the minimum on/off times constraints are satisfied. The pulse width request $t_{PW}^{request}$ used as input to this logic is first defined based on a chosen average-time interval t_{av} and the resulting duty cycle D_c, i.e.

$$t_{PW}^{request} = D_c t_{av}, \quad D_c = \frac{P_{NBI}}{P_{NBI}^{max}}. \tag{17}$$

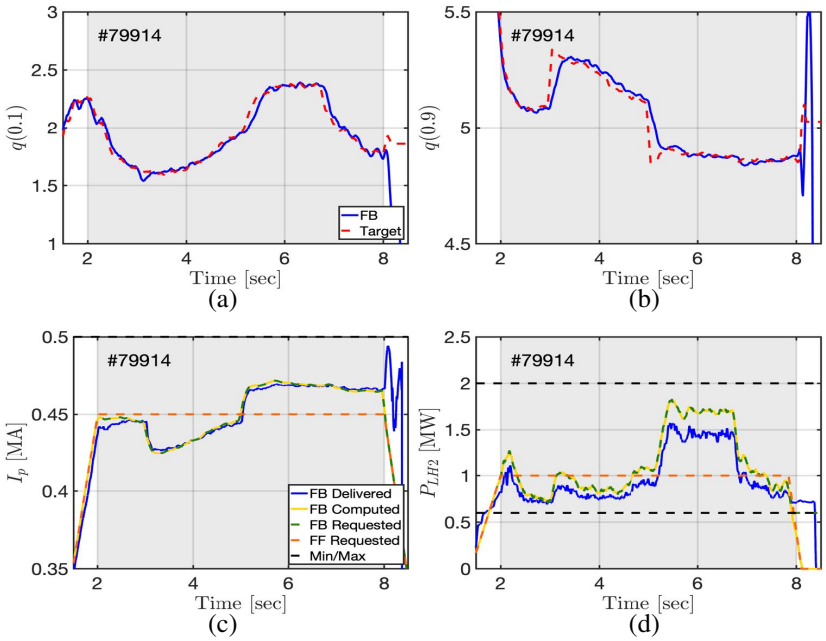

Figure 4: *Time evolutions of the q profile at (a) $\hat{\rho} = 0.1$, (b) $\hat{\rho} = 0.9$. The targets (dashed-red lines) are compared with the actual values (solid-blue lines) for the FF+FB shot #79914. Time evolutions for (c) plasma current, (d) 4.60 GHz LHW source power are shown for this shot. The dashed-orange lines show the FF component of the computed actuation. The solid-yellow, dashed-green and solid-blue lines show the computed (before saturation), requested (after saturation), and delivered actuations, respectively, for the overall FF+FB actuation in shot #79914. Saturation levels are denoted by dashed-black lines.*

4.6. Simulation Simserver

Simserver is a valuable tool in two aspects. First, it enables the debugging of the implementation of the Profile Control category, and, second, it validates the computations carried out by the implemented control algorithm before experimental testing. The configuration of the Simserver is given in Fig. 2(c). It runs closed-loop simulations coupling the PCS and a simulator when the test switch selects the testing mode. The simulator in this work is a Matlab®/Simulink® *S-function* containing the plasma-response model introduced in Section 2. The input/output structure of the simulator is made consistent with the input/output structure of the EAST PCS.

5. Experimental Results

Fig. 4 shows feedback regulation of the q profile at two points in space, namely $q(\hat{\rho} = 0.1)$ and $q(\hat{\rho} = 0.9)$, by using the ohmic coils and the high-frequency (4.60 GHz) LHW source as actuators for EAST shot #79914. The target evolutions for the q profile at these two points, which have been obtained from a previous shot to ensure feasibility, are shown in dashed-red lines in Fig. 4(a) and Fig. 4(b). The requested plasma current and 4.60 GHz LHW power determined by the q-profile feedback controller are shown respectively by the dashed green lines in Fig. 4(c) and Fig. 4(d). When feedback control is turned on in shot #79914 for 2s< t <8s, the feedforward-control components shown by the dashed-orange lines in both figures are corrected to produce the actuation shown by the dashed-green lines, which is needed to successfully track the targets as noted by comparing solid-blue and dashed-red lines in Fig. 4(a) and Fig. 4(b). In spite of the bias between requested and delivered LHW power (dashed-green vs solid-blue lines), the q-profile feedback controller (11) is capable of tracking the targets due to the presence of integral action. The bias between requested and delivered power in the LHW source respond to the way it is controlled by the associated actuator category. The actuation requested by the q-profile feedback controller, shown in dashed-green lines in the bottom figures, is the result of constraining the actuation computed by the controller, shown in solid-yellow lines in the same figures, by the physical limits associated to the different actuators. These saturation limits, which are shown by dashed-black lines, were not active in this discharge.

Fig. 5 shows feedback regulation of the q profile at two points in space, namely $q(\hat{\rho} = 0.1)$ and $q(\hat{\rho} = 0.9)$, and β_N by using the ohmic coils, the high-frequency (4.60 GHz) LHW source, and the NBI1L beam as actuators for EAST shot #80221. The target evolutions for both the q profile at these two points and β_N have once again been obtained from a previous shot to ensure feasibility. These targets are shown in dashed-red lines in Fig. 5(a), Fig. 5(b), and Fig. 5(c). When feedback control is turned on in shot #80221 for 2s< t <8s, the feedforward-control components of the actuation shown by the dashed-orange lines in Fig. 5(d), Fig. 5(e), and Fig. 5(f) are corrected by the feedback control algorithm to produce the actuation shown by the dashed-green lines, which is needed to successfully track the targets. The actuation requested by the q-profile+β_N feedback controller (dashed-green

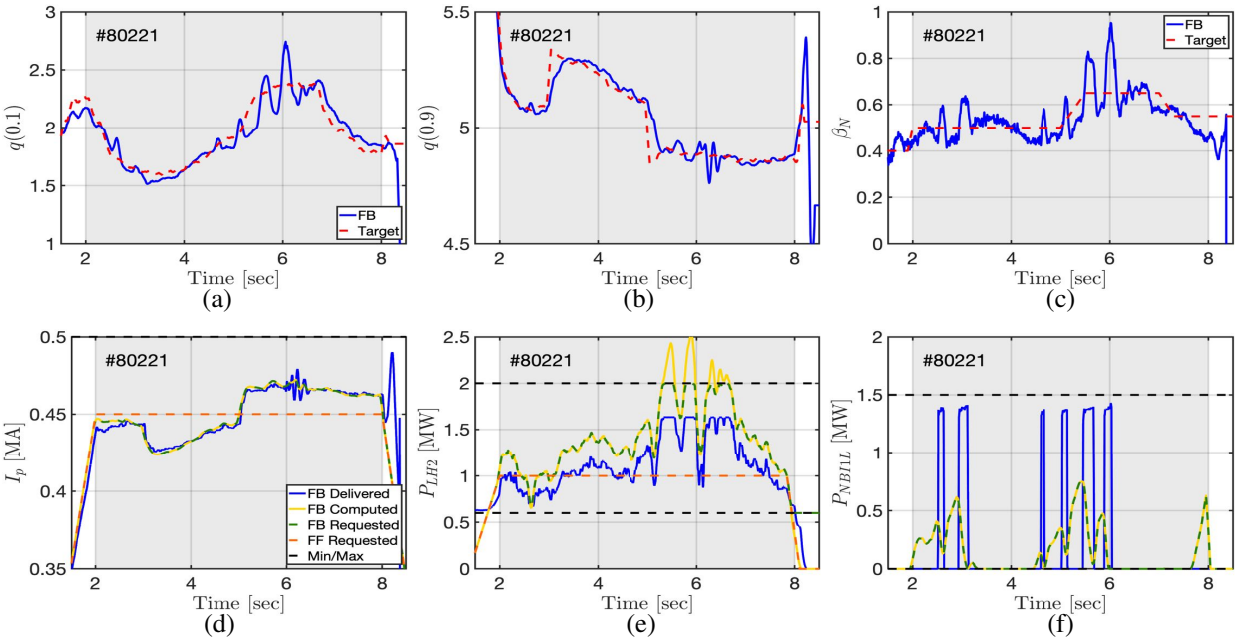

Figure 5: *Time evolutions of the q profile at: (a) $\hat{\rho} = 0.1$, (b) $\hat{\rho} = 0.9$, and (c) β_N. The targets (dashed-red lines) are compared with the actual values (solid-blue lines) for the FF+FB shot #80221. Time evolutions for: (d) plasma current, (e) 4.60 GHz LHW source power, (f) NBI1L source power are shown for this shot. The dashed-orange lines show the FF component of the computed actuation. The solid-yellow, dashed-green and solid-blue lines show the computed (before saturation), requested (after saturation), and delivered actuations, respectively, for the overall FF+FB actuation in shot #80221. Saturation levels are denoted by dashed-black lines.*

lines) is the result of constraining the actuation computed by the controller, shown in solid-yellow lines in the same figures, by the physical limits associated to the different actuators. These saturation limits, which are shown by dashed-black lines, were indeed active for the LHW source power. In this shot, the PWM algorithm introduced in Section 4.5 was used with mixed results to command the NBI1L source. As noted by comparing solid-blue and dashed-red lines in Fig. 5(a), Fig. 5(b), and Fig. 5(c), the targets are tracked in average but the PWM algorithm introduces significant perturbations due to both the minimum time-on and minimum time-off constraints significantly impacting this relatively low-β_N plasma and some detected implementation issues (feedforward control set to zero and unnecessary time delay introduced by the PWM algorithm). Once again, a bias is observed between the requested and delivered power in the LHW source due to the way it is controlled by the associated actuator category. Nevertheless, the q-profile+β_N feedback controller (11) is capable of tracking the targets in spite of the perturbations introduced by the PWM algorithm due to the presence of integral action.

Fig. 6 shows feedback regulation of the q profile at three points in space, namely $q(\hat{\rho} = 0.1)$, $q(\hat{\rho} = 0.5)$, $q(\hat{\rho} = 0.9)$, by using the ohmic coils, the low-frequency (2.45 GHz) LHW source, and the high-frequency (4.60 GHz) LHW source as actuators for EAST shot #95183. The target evolutions for the q profile at these three points, which once again have been obtained from a previous shot to ensure feasibility, are shown in dashed-red lines in Fig. 6(a), Fig. 6(b) and Fig. 6(c). The solid-magenta lines show the evolutions of the q profile at these points for feedforward-only EAST shot #95176. The feedforward actuation for the plasma current, the 2.45 GHz LHW power, and the 4.60 GHz LHW power, shown respectively in Fig. 6(d), Fig. 6(e) and Fig. 6(f) by the solid-magenta lines, is not adequate enough to track the desired targets. This can be appreciated from Fig. 6(a), Fig. 6(b) and Fig. 6(c), where the associated feedforward-only evolutions of the q profile are also shown by solid-magenta lines. When feedback control is turned on in shot #95183 for 2s$< t <$8s, the actuation is corrected to successfully track the targets as shown by the solid-blue lines in the same top figures. The feedforward-only actuation is corrected in this case by the feedback controller to produce the actuation shown also by solid-blue lines in the bottom figures. In spite of the bias between requested and delivered power from the two LHW sources (dashed-orange vs. solid-magenta lines for the feedforward-only shot, dashed-green vs solid-blue lines for the feedforward+feedback shot), the q-profile feedback controller (11) is capable of tracking the targets due to the presence of integral action. The actuation requested by the q-profile feedback controller, shown in dashed-green lines in the bottom figures, is the result of constraining the actuation computed by the controller, shown in solid-yellow lines in the same figures, by the physical limits associated to the different actuators. These limits are shown by dashed black lines in the figures. An anti-windup augmentation of the controller is in place to prevent the windup of the controller's state due to integral action during the occurrence of actuator saturation and to therefore preserve the tracking performance. Around 1MW of Electron Cyclotron Range of Frequency (ECRF) H&CD power was used in this shot to keep the plasma in H-mode.

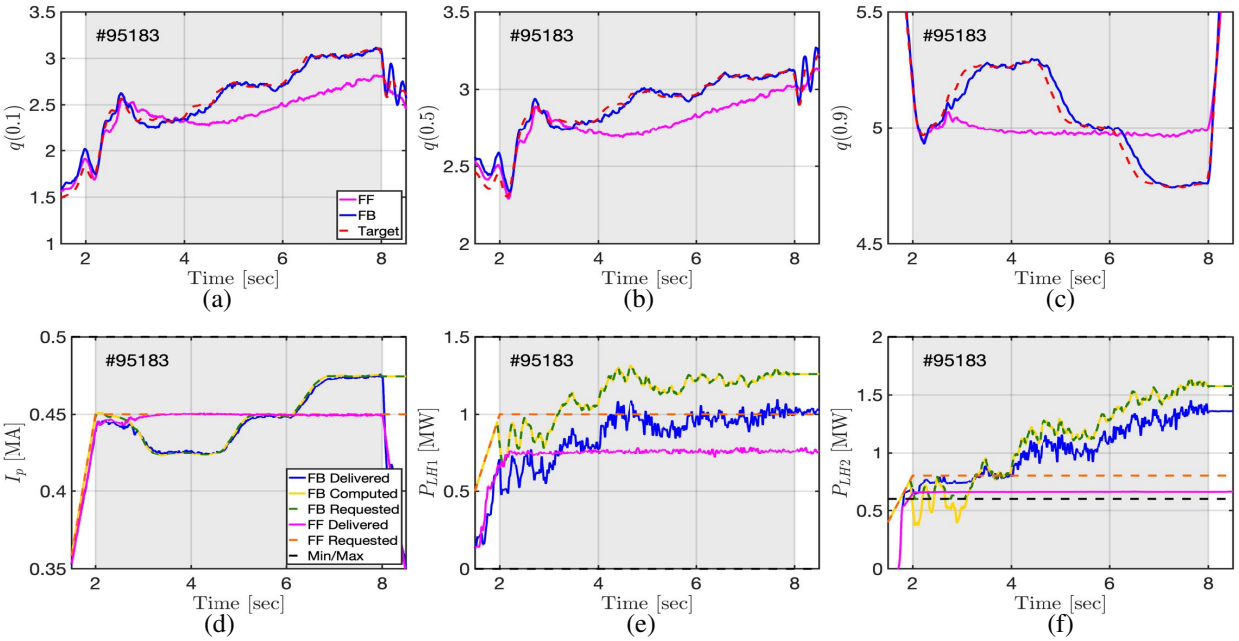

Figure 6: *Time evolutions of the q profile at: (a) $\hat{\rho} = 0.1$, (b) $\hat{\rho} = 0.5$, (c) $\hat{\rho} = 0.9$. The target (dashed-red line) is compared with a FF-only (solid-magenta line) shot (#95176) and a FF+FB (solid-blue line) shot (#95183). Time evolutions for: (d) plasma current, (e) 2.45 GHz LHW source power, (f) 4.60 GHz LHW source power are shown for both shots. The dashed-orange and solid-magenta lines show requested and delivered actuations for FF-only shot #95176. The solid-yellow, dashed-green and solid-blue lines show the computed (before saturation), requested (after saturation), and delivered actuations for FF+FB shot #95183. Saturation levels are denoted by dashed-black lines.*

6. Conclusion and Possible Future Work

Successful q-profile+β_N control was demonstrated for the first time in EAST. As the number of actuators is increased (by enhancing the NBI PWM algorithm and testing it in H-mode plasmas, and by incorporating the command of ECRF and Ion Cyclotron Range of Frequency (ICRF) H&CDs under the PCS), the quality of the real-time reconstruction is improved (by constraining pEFIT with POlarimeter-INTerferometer (POINT) measurements [10]), and the prediction accuracy of the control-level models used for control design is enhanced (by further developing control-physics understanding and continuing validation efforts), the capability of tightly regulating the q-profile and β_N will be further augmented in order to routinely enable the access to long-pulse, disruption-free, high-performance operation in EAST. It is anticipated that this augmented control capability will be achieved by employing more sophisticated, model-based, optimal, control algorithms.

Acknowledgments

Work supported by the U.S. Department of Energy, Office of Science, Office of Fusion Energy Sciences, under Awards DE-SC0010537 and DE-SC0010685, and by the National Magnetic Confinement Fusion Science Program of China under Award 2017YFE0301300.

Disclaimer

This report was prepared as an account of work sponsored by an agency of the US Government. Neither the US Government nor any agency thereof, nor any of their employees, makes any warranty, express or implied, or assumes any legal liability or responsibility for the accuracy, completeness, or usefulness of any information, apparatus, product, or process disclosed, or represents that its use would not infringe privately owned rights. Reference herein to any specific commercial product, process, or service by trade name, trademark, manufacturer, or otherwise, does not necessarily constitute or imply its endorsement, recommendation, or favoring by the US Government or any agency thereof. The views and opinions of authors expressed herein do not necessarily state or reflect those of the US Government or any agency thereof.

References

[1] H. Wang, E. Schuster et al., Model-based optimal scenario planning in EAST, Fusion Eng Des, **123**, 569 (2017)
[2] H. Wang and E. Schuster, Robust control of the current profile and plasma energy in EAST, Fusion Eng Des, **146**, 688 (2019)
[3] H. Wang, W. P. Wehner et al., "Combined Current Profile and Plasma Energy Control Via Model Predictive Control in the EAST Tokamak", in *2018 26th Mediterranean Conference on Control and Automation (MED)*, 1–9 (2018)
[4] Y. Huang, B. Xiao et al., Implementation of GPU parallel equilibrium reconstruction for plasma control in EAST, Fusion Eng Des, **112**, 1019 (2016)
[5] F. Hinton and R. Hazeltine, Theory of Plasma Transport in Toroidal Confinement Systems, Rev. Mod. Phys., **48**, 239 (1976)
[6] Y. Ou, T. Luce et al., Towards model-based current profile control at DIII-D, Fusion Eng. Des., **82**, 1153 (2007)
[7] J. Barton, W. Shi et al., "Physics-based Control-oriented Modeling of the Current Density Profile Dynamics in High-performance Tokamak Plasmas", in *52nd IEEE International Conference on Decision and Control* (2013)
[8] O. Sauter, C. Angioni et al., Neoclassical conductivity and bootstrap current formulas for general axisymmetric equilibria and arbitrary collisionality regime, Phys. Plasmas, **6**, 2834 (1999)
[9] ITER EDA et al., ITER Physics Basis Editors, Nucl. Fusion, **39**, 2201 (1999)
[10] Y. Huang, B. Xiao et al., Development of real-time plasma current profile reconstruction with POINT diagnostic for EAST plasma control, Fusion Eng Des, **120**, 1 (2017)